Facile, Large-Quantity Synthesis of Stable, Tunable-Color Silicon Nanoparticles and Their Application for Long-Term Cellular Imaging

Yiling Zhong, Xiaotian Sun, Siyi Wang, Fei Peng, Feng Bao, Yuanyuan Su, Youyong Li, Shuit-Tong Lee,* and Yao He*

Jiangsu Key Laboratory for Carbon-Based Functional Materials and Devices, Institute of Functional Nano and Soft Materials (FUNSOM), Soochow University, Suzhou 215123, China

ABSTRACT We herein introduce a facile, low-cost photochemical method capable of rapid (<40 min) and large-quantity (~10 g) production of highly fluorescent (quantum yield: 25%) silicon nanoparticles (SiNPs) of tunable optical properties (peak emission wavelength in the range of 470−560 nm) under ambient air conditions, by introducing 1,8-naphthalimide as a reducing agent and surface ligands. The as-prepared SiNPs feature robust storage stability and photostability preserving strong and stable fluorescent during long-term (>3 h) high-power UV irradiation, in contrast to the rapid fluorescence quenching within 2 h of conventional organic dyes and II−VI quantum dots under the same conditions. The as-prepared SiNPs serving as photostable nanoprobes are workable for cellular imaging in long-term manners. Our findings provide a powerful method for mild-condition and low-cost, large-quantity production of highly fluorescent and photostable SiNPs for various promising applications.

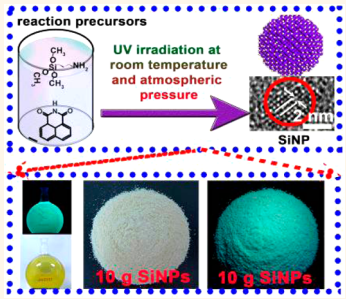

KEYWORDS: silicon nanoparticles · photochemical · large-quantity · long-term · bioimaging

Silicon nanomaterials hold great promise for wide-ranging optoelectronic and biotechnological applications because of their several unique merits including excellent optical/mechanical/electronic properties, facile surface modification, and compatibility with silicon technologies, *etc.*[1−23] Notably, Sailor *et al*. reported that SiNPs could be biodegradable *in vivo* in a relatively short period of time (~8 h) and the biodegraded product, orthosilicic acid, is biocompatible with numerous tissues and readily cleared *via* renal clearance.[5,17] In a recent study of the biodistribution of SiNPs in a healthy mouse, Prasad *et al*. found that SiNPs are prone to be degraded in the liver and spleen after two months.[23]

It is also worthwhile to point out that silicon nanoparticles (SiNPs) can yield strong fluorescence at small sizes (diameter equal to or smaller than ~5 nm) due to indirect-to-direct band gap transitions arising from a quantum-size confinement effect. For widespread applications of SiNPs, it is essential to be able to facilely prepare fluorescent SiNPs in large quantity at low cost and mild conditions. While different synthetic methods of SiNPs (*e.g.*, solution-phase reductive strategy, laser ablation, mechanochemical method, plasma-assisted aerosol precipitation, sonochemical synthesis, microemulsion, and microwave irradiation, *etc.*[6−13]) have been developed, they invariably require complicated procedures, harsh experiment conditions, and/or costly equipment (please see a detailed comparison of these methods in Supporting Information, Table S1). Recently, we introduced a microwave-assisted method capable of preparing ~0.1 g of fluorescent SiNPs in 10 min reaction. However, the synthesis required high temperature (~160 °C), high pressure (~10−15 times atmospheric pressure), and costly microwave equipment.[9] Despite the extensive efforts, rapid and low-cost mass production of highly fluorescent SiNPs under mild conditions remains unavailable.

We herein introduce a mild-condition, low-cost photochemical strategy capable of large-quantity synthesis of fluorescent

* Address correspondence to apannale@suda.edu.cn, yaohe@suda.edu.cn.

Received for review January 30, 2015 and accepted May 30, 2015.

Published online May 31, 2015
10.1021/acsnano.5b00683

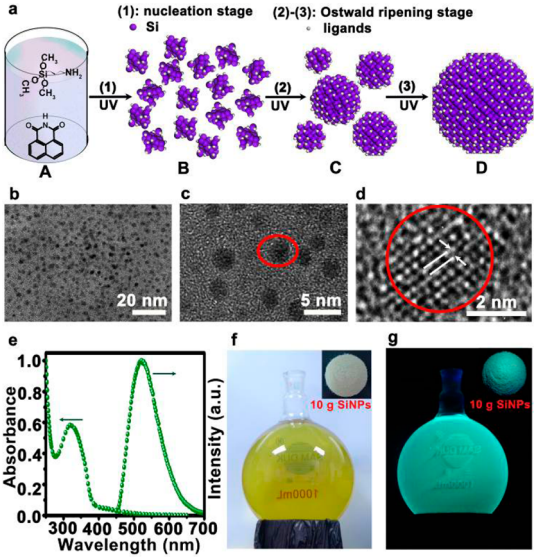

Figure 1. Schematic illustration of synthesis and characterization of SiNPs. (a) Illustration of the preparation of fluorescent SiNPs: (A) reaction precursors; (B) 16 nuclei; (C) 5 small-sized, and (D) 1 large-sized silicon nanocrystals. (b,c) TEM images of the resultant SiNPs. (d) HRTEM image of a SiNP indicated by a circle in panel c. (e) UV-PL spectra of the SiNPs. Images of 1 L aqueous solution dispersed with 10 g green-emitting SiNPs under ambient light (f) or 365 nm irradiation (g). Inset is a photograph showing 10 g of a green-emitting SiNPs sample under ambient light (f) or 365 nm irradiation (g).

SiNPs with robust storage-/photostability and tunable optical properties (*e.g.*, fluorescent intensities and peak emission wavelengths (λ_{max})). Specifically, the present synthesis can facilely and rapidly produce ~10 g fluorescent SiNPs in 40 min *via* one-pot reaction in inexpensive and common glass flasks performed under UV irradiation at room temperature (20−25 °C) and atmospheric pressure. The fluorescent yield (QY) of the as-prepared SiNPs can reach ~25% dependent on ligand concentrations, and the fluorescent color λ_{max} is tunable in the range of 470−560 nm. The resultant SiNPs are further employed as high-performance fluorescent biological probes for long-term cellular imaging application, preserving bright and stable fluorescent signals during 2 h continuous confocal observation.

RESULTS AND DISCUSSION

Photochemical Synthesis of Fluorescent SiNPs. As schematically illustrated in Figure 1a, the synthesis first involves reduction of (3-aminopropyl)trimethoxysilane ($C_6H_{17}NO_3Si$, APS) molecules by 1,8-naphthalimide ($C_{12}H_7NO_2$) molecules under UV irradiation to yield crystal nuclei (step 1: A → B, also see a proposed mechanism in Supporting Information, Figure S1).[24−26] When sufficient crystal nuclei are produced, the Ostwald ripening stage is triggered in the following reaction steps. Particularly, at the beginning of Ostwald ripening stage, growth of crystal nuclei leads to production of silicon nanocrystals of small sizes (step 2: B → C). As the Ostwald ripening stage continues, further nanocrystal growth occurs at the expense of dissolution of unstable nanocrystals featuring small sizes. As a result, larger-size silicon nanoparticles, which are more stable due to smaller surface-to-volume ratio than small-size nanocrystals, are formed in the third step.[27−29] Remarkably, the whole procedure is rapidly completed in less than 40 min in a common glass flask under UV irradiation at room temperature (20−25 °C) and atmospheric pressure without requiring harsh conditions and expensive instruments (See detailed description in the Experimental Section). Furthermore, the process can in principle be scaled up to produce any desirable amount of SiNPs by using appropriately larger amount of reactants. In Figure 1b−d, the transmission electron microscopy (TEM) and high-resolution TEM (HRTEM) images show that the prepared SiNPs assume a spherical structure with good monodispersity (Figure 1b), with lattice planes (220) of ~0.19 nm spacing in the HRTEM image (Figure 1d) revealing the crystallinity of the resultant SiNPs. Additional HRTEM/electron diffraction (Supporting Information, Figures S4, S6, S8) and X-ray diffraction (Figure 4) results provide convincing evidence that SiNPs are crystalline in nature. Figure 1e displays the normalized UV−vis photoluminescence (PL) spectra of the resultant SiNPs, showing resolved absorption peak and symmetrical PL peak. Note that our method is capable of rapid mass-production of SiNPs with strong fluorescence. In a typical experiment, 102.7 g of $C_6H_{17}NO_3Si$ and 20 g of $C_{12}H_7NO_2$ are dispersed in 1 L of water to serve as reaction precursors. Under 30 min of continuous UV irradiation at 365 nm, the reaction solution exhibits strong green fluorescence, indicating generation of fluorescent SiNPs. The resultant solution is purified *via* centrifugation and dialysis to remove residual reactants (*i.e.*, APS and 1,8-naphthalimide), and then dried and weighted, finally yielding ~10 g of green-emitting SiNPs (inset in Figure 1 panels f and g, see experiment details in Experimental Section). The as-prepared SiNPs are readily redispersed in water to yield a transparent solution (Figure 1f), which exhibits intense green fluorescence under UV irradiation (Figure 1g), demonstrating excellent water dispersibility of the as-prepared SiNPs due to a large amount of surface-covered hydrophilic amino groups.[6−11,30,31]

Tunable Fluorescent Intensities of SiNPs. The QY value of the as-prepared SiNPs is sensitively dependent on the concentration of 1,8-naphthalimide. In our experiment, 2, 4, 6, 8, 10, or 15 g of 1,8-naphthalimide is added to 1 L of aqueous solution containing 102.7 g of $C_6H_{17}NO_3Si$, respectively. With an increasing amount of 1,8-naphthalimide, the fluorescent intensity of the resultant solution after 30 min of reaction is increasingly enhanced (Figure 2a). Figure 2b presents the respective QY values of the six samples. It shows the QY value increases with increasing concentration of

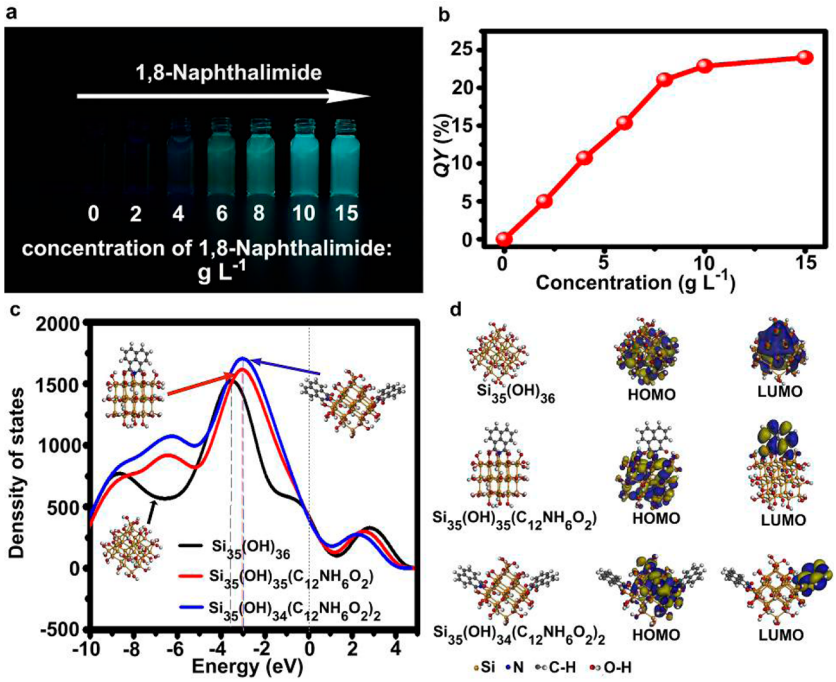

Figure 2. Optical properties of SiNPs synthesized from different concentrations of 1,8-naphthalimide. (a) Photographs of SiNPs under 365 nm irradiation (left) or ambient light (right). (b) QY of SiNPs prepared using 1,8-naphthalimide of different concentrations (0, 2, 4, 6, 8, 10, and 15 g/L, respectively). (c) Calculated density of states of a SiNP capped with one or two 1,8-naphthalimide molecules. (d) Isosurfaces of HOMO and LUMO orbitals in ground state configurations of $Si_{35}(OH)_{36}$, $Si_{35}(OH)_{35}(C_{12}NH_6O_2)$, and $Si_{35}(OH)_{34}(C_{12}NH_6O_2)_2$.

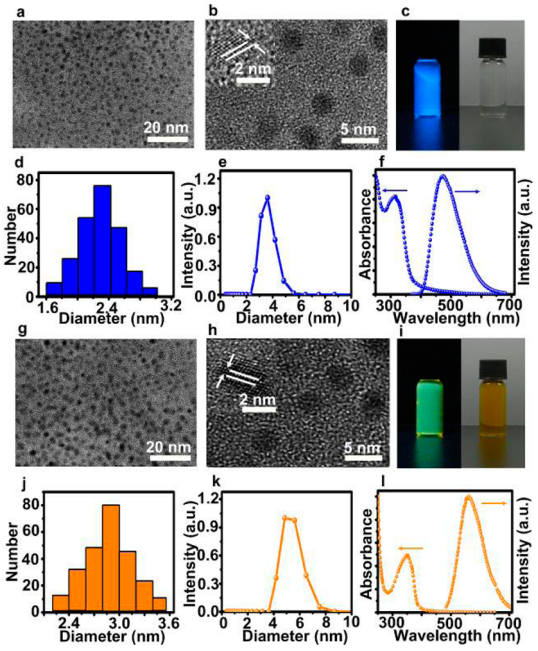

Figure 3. Characterization of blue- and light-green-emitting SiNPs. TEM and HRTEM images of the blue- (a, b) and light-green- (g, h) emitting SiNPs. Insets in panels b and h present the enlarged HRTEM images of a single blue- and light-green-emitting SiNP, respectively. Panels c and i present the photographs of blue- and light-green-emitting SiNPs under 365 nm irradiation (left) or ambient light (right). Panels d and j show the TEM diameter distribution of blue- and light-green-emitting SiNPs; panels e and k display DLS histograms of blue- and light-green-emitting SiNPs; panels f and l present UV-PL spectra of the blue- and light-green-emitting SiNPs.

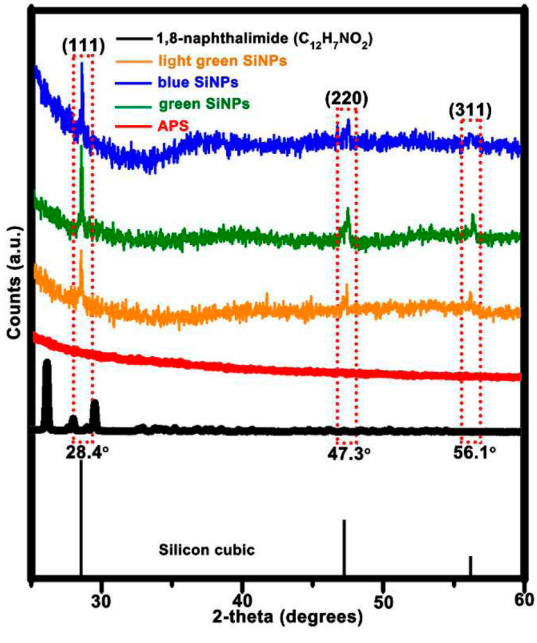

Figure 4. XRD patterns of the SiNPs, 1,8-naphthalimide ($C_{12}H_7NO_2$), and APS samples. The diffraction peaks are analyzed by commercial XRD software (PCPDFWIN). The standard diffraction lines of cubic silicon are also shown for comparison.

1,8-naphthalimide from ~2, 4, 6, 8, 10, to 15 g/L. Note that the surface of the as-prepared SiNPs is modified with 1,8-naphthalimide molecules containing a large amount of delocalized electrons, which would facilitate recombination of electrons and holes. As a result, the

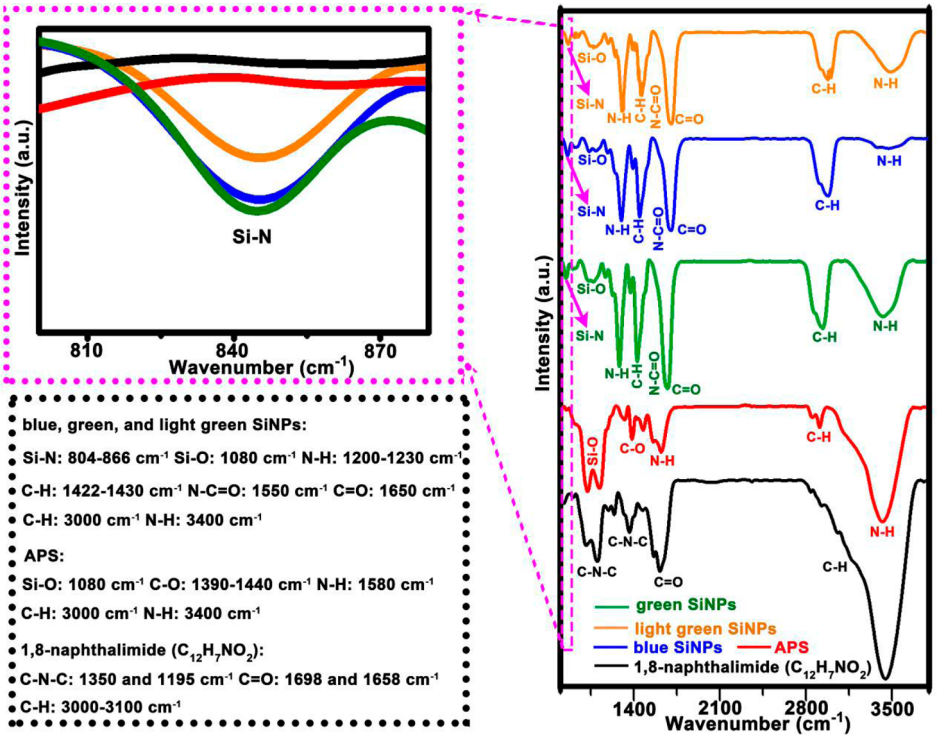

Figure 5. FTIR spectra of the SiNPs, 1,8-naphthalimide, and APS, exhibiting obvious absorption peaks at 800−3800 cm^{-1}.

QY value reaches as high as ~25% at ~15 g/L of 1,8-naphthalimide.[32−38] To understand the increase of QY of SiNPs with 1,8-naphthalimide, we perform density-functional tight-binding (DFTB) (Software for calculation: Material studio 6.0)[39,40] calculations of SiNPs (we simplify SiNP as $Si_{35}(OH)_{36}$ for convenient calculations). Figure 2c presents the calculated density of states of a SiNP capped with different numbers of 1,8-naphthalimide molecules (*i.e.*, 0, 1, and 2, indicated by $Si_{35}(OH)_{36}$, $Si_{35}(OH)_{35}(C_{12}NH_6O_2)$, and $Si_{35}(OH)_{34}(C_{12}NH_6O_2)_2$, respectively). It shows that the attachment of 1,8-naphthalimide to the surface of $Si_{35}(OH)_{36}$ introduces new gap states in SiNP. As a result, more electrons can be transferred from the lowest unoccupied molecular orbitals (LUMOs) to the new gap states or highest occupied molecular orbitals (HOMOs), thereby leading to substantive enhancement of PL intensity. With more 1,8-naphalimide molecules attached to SiNP, the enhancement effect is increasingly larger. Similar results have been previously reported by our group.[41,42] The isosurfaces of HOMO and LUMO orbitals in the ground state configurations of $Si_{35}(OH)_{36}$, $Si_{35}(OH)_{35}(C_{12}NH_6O_2)$, and $Si_{35}(OH)_{34}(C_{12}NH_6O_2)_2$ are shown in Figure 2d. For $Si_{35}(OH)_{36}$, both HOMO and LUMO are delocalized throughout the core of the silicon cluster. In contrast, for 1,8-napthalimide molecules-capped SiNP (*e.g.*, $Si_{35}(OH)_{35}(C_{12}NH_6O_2)$ and $Si_{35}(OH)_{34}(C_{12}NH_6O_2)_2$), while the HOMO remains delocalized in the silicon cluster, the LUMO is distributed on the 1,8-naphalimide molecule. Therefore, the excited-state charge transfer (CT) process would occur between the delocalized electrons of surface-covered 1,8-naphalimide (serving as ligand and donor) and excitons of SiNP (serving as core and acceptor), resulting in substantive improvement of the PL intensity.[35−38]

Tunable Fluorescent Color of SiNPs. The present method can easily tune the peak fluorescent wavelength of SiNPs *via* adjustment of reaction time. Typically, 30 min UV irradiation produces ~10 g of green-emitting SiNPs (see Figure 1 and corresponding discussion), while 15 or 40 min irradiation, respectively, gives ~10 g of blue- or light-green-emitting SiNPs (note that except for the irradiation time, all other conditions, such as reactant concentrations, are the same). Figure 3 panels a and b display the TEM and HRTEM images of blue-emitting SiNPs, showing that the resultant spherical SiNPs possess good monodispersity and high crystallinity, with (220) lattice planes of ~0.19 nm. As displayed in Figure 3c, the resultant SiNPs exhibit distinctly blue fluorescence (with a QY of ~25%) under UV irradiation and are well dispersed in water with high transparency. We also calculate over 200 SiNPs to measure the size distribution of SiNPs as 2.3 ± 0.5 nm, which is slightly smaller than that (~3.6 nm) determined through dynamic light scattering (DLS, Figure 3e), resulting from various tested conditions in TEM and DLS characterizations.[43−45] The UV-PL spectra of the blue-emitting SiNPs, as presented in Figure 3f, exhibit resolved absorption and symmetrical photoluminescence peaks. Similarly, the light-green-emitting SiNPs feature strong fluorescence (with QY of ~25%), good monodispersibility, and excellent crystallinity

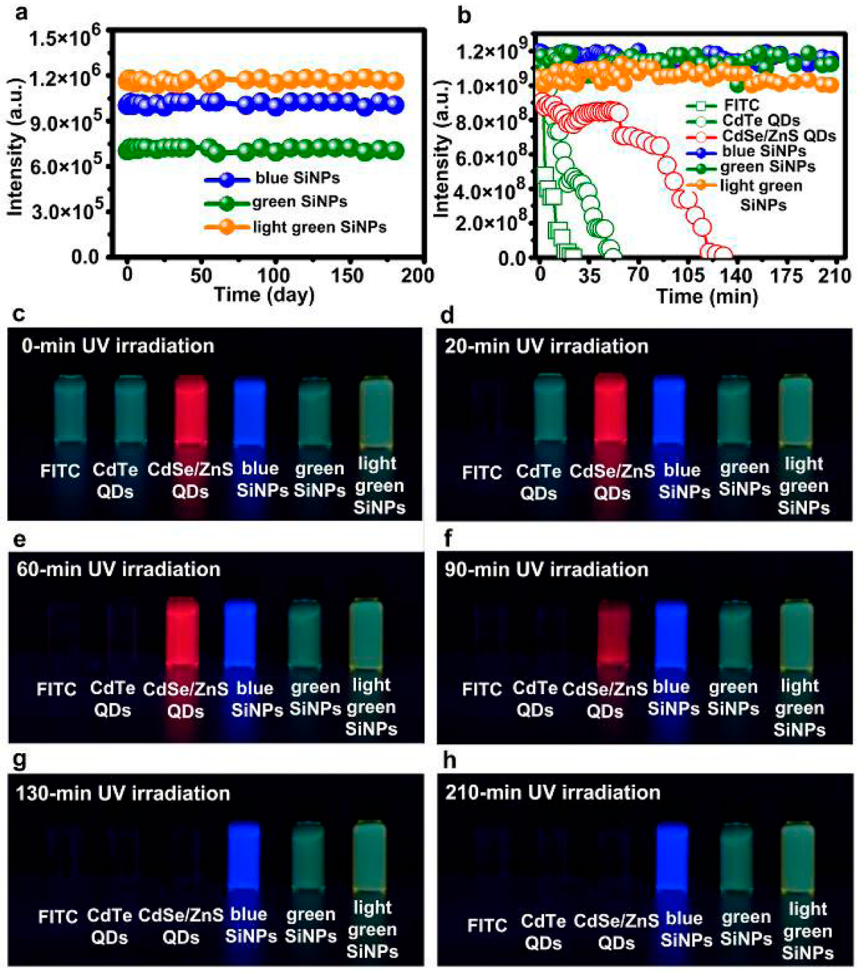

Figure 6. Optical properties of SiNPs. (a) The as-prepared aqueous samples of SiNPs retain nearly identical fluorescent intensity during 180-day storage. (b) Photostability comparison and (c−h) photographs of aqueous solutions of FITC, CdTe QDs, CdSe/ZnS QDs, and three different-color SiNPs under continuous UV irradiation (450 W xenon lamp) for serial times.

(Figure 3g−i). Compared to the blue-emitting SiNPs, the light-green-emitting SiNPs are larger in diameter (*i.e.*, 2.8 ± 0.6 nm by TEM; 5.2 nm by DLS), which significantly contributes to the observed red shift of emission wavelengths (*e.g.*, the quantum-size confinement effect induces a band gap decrease of SiNPs with increasing particle size, resulting in a redshift in fluorescence and absorption energy).[46−48]

XRD and FTIR Characterization of SiNPs. Systematic characterizations including powder X-ray diffraction (XRD) was also performed, convincingly demonstrating that the as-prepared SiNPs are responsible for the observed distinct blue, green, and light-green fluorescence. As displayed in Figure 4, the XRD spectrum of the 1,8-naphthalimide ($C_{12}H_7NO_2$) features characteristic and sharp diffraction peaks at 26.3°, 28.1°, 29.7°, *etc* (black line). The XRD patterns of APS (red line) characteristically show no sharp diffraction peaks. In comparison, the resultant SiNPs samples exhibit three standard diffraction peaks (blue, green, and yellow lines) at 28.4° (111), 47.3° (220), and 56.1° (311). Taken together TEM/HRTEM results reveal ultrasmall size of SiNPs (diameter: ~1.8−3.4 nm), and we deduce the quantum confinement effects and high crystallization as two significant contributors to the observed blue, green, and light-green fluorescence, well consistent with previous reports.[6−13,49−52]

FTIR spectra of the SiNPs, 1,8-naphthalimide, and APS are further measured in our experiment, exhibiting obvious absorption peaks at 800−3800 cm^{-1} (Figure 5). In particular, for 1,8-naphthalimide (black line), the characteristic FTIR peaks for the C−N−C imide group from 1,8-naphthalimide moiety locate at 1195 and 1350 cm^{-1}. The stretching frequencies bands $\nu_{C=O}$ absorption are observed with very strong intensity bands at 1698 and 1658 cm^{-1}. The stretching vibration of the −CH aromatic are observed at 3000−3100 cm^{-1} (black line). For APS (red line), the strong FTIR absorbance peaks at 1080, 1390−1440, 1580, 3000, and 3400 cm^{-1} are assigned to the vibrational stretch of Si−O bonding, C−O vibration, N−H bending vibrations, C−H vibration, and the N−H stretching vibration, respectively. For the three-color luminescent SiNPs (green, yellow, and orange lines), the strong FTIR

absorbance peaks at 1080, 1200−1230, 1422−1430, 1550, 1650, 3000, and 3400 cm^{-1} are assigned to the vibrational stretch of Si−O bonding, N−H deformation vibration, the C−H aromatic skeletal vibration, N−C═O vibration, C═O stretching vibration, C−H vibration, and the N−H stretching vibration, respectively. For a clear comparison, the enlarged spectra ranging from 800 to 880 cm^{-1} are shown in the pink frame. Typically, FTIR spectra of 1,8-naphthalimide and APS show feeble absorbance peaks. In sharp contrast, we can clearly see the distinct absorptions at 804−866 cm^{-1} which are ascribed to the vibrational stretch of Si−N bonding, confirming the existence of Si−N bonds in the as-prepared SiNPs.[9,53−60]

Ultrahigh Storage and Photostability of SiNPs. Notably, the as-prepared SiNPs preserve extremely stable optical properties during long-term storage and high-power UV irradiation. Specifically, the as-prepared blue-, green-, and light-green-emitting SiNPs maintain identical UV-PL spectra, maintaining high and stable PL intensity during 180-day storage in ambient environment (Figure 6a and Supporting Information, Figures S15−S17). We compare photostability of the as-prepared three-color SiNPs with the well-established II−VI quantum dots (QDs) and FITC (one kind of conventional organic dyes). Figure 6b shows that the fluorescent signals of FITC rapidly quench during 10 min of UV irradiation. Comparatively, CdTe QDs preserve over 50% of the original fluorescent intensity during 25 min of UV treatment, but their fluorescence becomes negligible in 50 min owing to Te oxidation under high-power UV irradiation.[14−17,61,62] For CdSe/ZnS core−shell QDs with higher photostability compared to CdTe QDs, their fluorescence is reduced to 50% in 90 min and becomes undetectable in 130 min because of UV irradiation-induced surface deterioration.[63] In marked contrast, the multicolor SiNPs are strikingly stable, for which the fluorescence intensities keep nearly unchanged during 210 min of UV irradiation, which is due to the unique photoluminescence features of SiNPs.[6−11] Figure 6 panels c−h present typical photographs of the above-mentioned six samples irradiated by UV light for different times. For the samples of FITC (Figure 6d), CdTe QDs (Figure 6e), and CdSe/ZnS QDs (Figure 6g), their fluorescence is distinct in the beginning of UV irradiation, but gradually vanish as irradiation time increases. Severe fluorescence quench happens within 20, 60, and 130 min of UV irradiation, respectively. In striking contrast, all three multicolor SiNPs samples maintain stable and bright fluorescence during 210 min of irradiation (Figure 6c−h), demonstrating the exceptional photostability of the as-prepared SiNPs. In addition to strong fluorescence and high photo/storage-/pH-stability (*e.g.*, the as-prepared SiNPs also maintain stable fluorescence in the pH range of 4−10, Supporting Information, Figures S21 and S22), the as-prepared

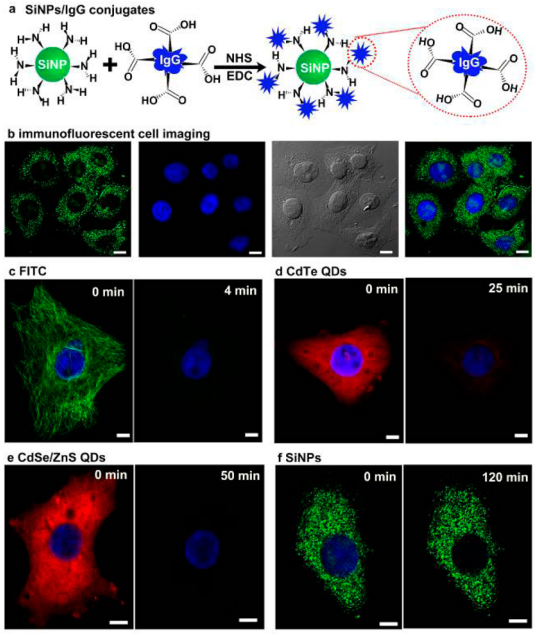

Figure 7. SiNPs/IgG conjugates and cell imaging photos captured by laser scanning confocal microscopy. (a) Schematic illustration of conjugation of SiNPs with goat-antimouse IgG. (figure not to scale). (b) (Left) microtubules of Hela cells are labeled by the IgG-conjugated SiNPs (excitation, 488 nm; detection window, 500−600 nm); (middle) cellular nuclei are imaged by Hoechst (excitation, 405 nm; detection window, 415−485 nm); (right) superposition of the two fluorescence images. (c−f) Temporal evolution of fluorescent signals of FITC, CdTe QDs, CdSe/ZnS QDs, Hoechst, and SiNPs. Scale bars: 10 μm. The green-emitting SiNPs were employed as a model.

SiNPs exhibit little or no cytotoxicity during 48 h of incubation with cells attributable to favorable biocompatibility of silicon (Figure S23).

SiNPs/IgG Conjugates and Immunofluorescent Cell Imaging. Taking advantages of strong fluorescence, ultrahigh photostability, and favorable biocompatibility, the as-prepared SiNPs are further employed as high-efficacy fluorescent bioprobes for bioimaging applications. In our experiment, the SiNPs are first conjugated with protein (*e.g.*, goat-antimouse IgG) *via* an established *N*-(3-(dimethylamino)propyl)-*N*′-ethylcarbodiimide hydrochloride (EDC)/*N*-hydroxysuccininmide (NHS)) cross-linking reaction (Figure 7a),[64,65] producing the SiNPs-IgG conjugates, which can serve as SiNPs bioprobes capable of cellular immunofluorescent labeling. Figure 7b displays cellular microtubules and nuclei that are stained by the SiNPs bioprobes (green signals) and a cell-nucleus dye Hoechst (blue signals), respectively. It is worth pointing out that such SiNPs bioprobes are superbly suitable for long-term cellular imaging. For systematic comparison, three control groups, namely, FITC (one kind of commercial organic dye), CdTe, and CdSe/ZnS quantum dots (QDs, well-studied photostable nanomaterials), are used for cell imaging. Typically, the fluorescence of FITC is rapid bleached within 4 min of observation under

laser-scanning confocal fluorescent microscopy (Figure 7c). Comparatively, while the QDs are more photostable than FITC, their fluorescence is nevertheless undetectable in less than 1 h observation, since long-time UV irradiation would deteriorate the surface of QDs, leading to severe fluorescence quenching (Figure 7 panels d and e. Compared to CdTe QDs, CdSe/ZnS QDs possess better photostability due to protection of ZnS shell capped on their surface).[7−9] In striking contrast, the fluorescence of SiNPs remains bright and stable during 2 h of continuous observation (Figure 7f), suggesting the SiNPs are suitable bioprobes for long-term bioimaging.

CONCLUSIONS

In summary, we report a mild-condition and low-cost photochemical synthetic method capable of large-quantity production of highly fluorescent and stable SiNPs. Compared to prior work (Supporting Information, Table S1), the present method is highly attractive as the prepared SiNPs exhibit superior properties and performance to all previous SiNPs. Our method can facilely produce ∼10 g of blue-, green-, and light-green-emitting SiNPs in 15-, 30-, and 40 min of UV irradiation, respectively, at room temperature (20−25 °C) and ambient pressure, and can in principle be scaled up at ease to produce larger quantities of SiNPs. The fluorescent quantum yield and color of the as-prepared SiNPs can be readily tuned, respectively, *via* varying ligand concentration and reaction time. SiNPs with high QY (∼25%) and tunable emission peak (∼470 to 560 nm) are readily produced. The SiNPs can serve as high-performance nanoprobes capable of highly efficacious, long-term immunofluorescent cell imaging. Given the facile, rapid, and low-cost attributes of the present synthesis, the resultant highly fluorescent SiNPs of tunable color, high storage stability, and photostability should hold great promise for wide-ranging biological and optoelectronic applications, including bioimaging, sensing, light-emitting diodes, and solar cells, *etc.*[14−23,66−68]

EXPERIMENTAL SECTION

Materials and Devices. (3-Aminopropyl)trimethoxysilane (APS) (97%) and 1,8-naphthalimide were purchased from Sigma-Aldrich. CdSe/ZnS QDs were bought from Wuhan Jiayuan Co., Ltd. (China). All chemicals were used as received. Milli-Q water (Millipore) was used as the solvent for preparing solutions. The 450 W xenon lamp with 365 nm ultraviolet light was supplied by Spectroline, USA. The SiNPs were characterized by transmission electronic microscopy (TEM), high-resolution TEM (HRTEM), UV−vis absorption, photoluminescence (PL), X-ray power diffraction (XRD), X-ray photoelectron spectra (XPS), and Fourier-transform infrared (FTIR) spectroscopy. A PerkinElmer Lambda 750 UV−vis−infrared spectrophotometer equipped with exclusive quartz cuvettes was used for recording UV−vis absorption spectra. A Horiba Jobin Yvon Fluoromax-4 spectrofluorimeter equipped with exclusive quartz cuvettes is utilized for recording PL spectra (excitation wavelength = 420 nm). A Philips CM 200 electron microscope (200 kV) was employed for capturing the TEM/HRTEM images. A DynaPro dynamic light scatterer (DLS) was used for performing DLS measurements (temperature, 25 °C; scan times, 100; dispersant, water; RI, 1.330; viscosity, 0.08872 cP; dielectric constant, 78.5). A Bruker Hyperion FTIR spectrometer was employed for recording FTIR spectra (32 scans; resolution, 4 cm^{-1}). A Panalytical Empyrean X-ray diffractometer was used for recording power X-ray diffraction (XRD) spectra (40 mA, 40 kV). A Philips CM 200 electron microscope equipped with EDX spectroscopy was utilized for recording energy-dispersive X-ray (EDX) spectroscopy.

Experimental Procedure. *Photochemical Synthesis of Fluorescent SiNPs.* The SiNPs precursor solution was synthesized through the addition of 100 mL of APS to 900 mL of Milli-Q water dispersed with 20 g of 1,8-naphthalimide. The mixture was thoroughly stirred for 10 min. The multicolor fluorescent SiNPs were prepared under different experimental conditions (*e.g.*, reaction time). In our experiment, the reaction time for producing blue-, green-, and light green-emitting SiNPs was 15, 30, and 40 min, respectively. After UV irradiation, the as-prepared SiNPs sample was collected after cooling to lower than 30 °C naturally. To exclude the influence of residual reactants, 1,8-naphthalimide was first precipitated through centrifugation at 6000 rpm for 15 min. The resultant SiNPs and APS remained in clear supernatant since they would not precipitate at this low centrifugation rate. For example, SiNPs would not precipitate at even higher centrifugation rate (*e.g.*, 10 000 rpm) because of their low molecular weight. The clear supernatant solution containing the as-prepared SiNPs and APS was then collected and further purified by dialysis (MWCO, 1000, Spectra/Pro) against Milli-Q water to remove APS. The residual APS was fully filtrated because of their smaller molecular weight (<1 kDa). The SiNPs whose molecular weight is larger than 1 kDa were collected and further diluted by Milli-Q water. The purified SiNPs aqueous solution was dried and weighed, yielding ∼10 g of highly fluorescent SiNPs. Note that the produced ∼10 g of SiNPs is readily redispersed in 1 L of water.

Tunable Fluorescent Intensity of SiNPs. In our experiment, 2, 4, 6, 8, 10, or 15 g of 1,8-naphthalimide was added into 1 L aqueous solution containing 102.7 g of $C_6H_{17}NO_3Si$, respectively. The mixture was thoroughly stirred for 10 min. After 30 min of UV irradiation, the as-prepared green-emitting SiNPs sample was collected after cooling to lower than 30 °C naturally. The as-prepared green-emitting SiNPs were used for optical measurements. For the blue-, green-, and light green-emitting SiNPs, their PLQY values were determined using quinine sulfate in 0.1 M H_2SO_4 (QY: 58%), Rhodamine 6G (QY: 95%), and Rhodamine B (QY: 99%) in ethanol, respectively, as a reference standard, which was freshly prepared to reduce the measurement error.[9,69] In detail, the optical densities (OD) at the excitation wavelength of the referenced dyes and the as-prepared SiNPs were adjusted to the same values. To avoid reabsorption, the dominant absorption peak of organic dyes and the first exciton absorption peak of the SiNPs were required to be smaller than 0.1. The integrated PL intensities (*via* areas calculated form PL spectra) *vs* corresponding absorbance were plotted to yield two straight lines, whose gradients could be employed for determining the PLQY values based on the established equation: $Q_x = Q_r M_x N_x^2/(M_r N_r^2)$. *N*, *M*, and *Q* stand for the average refractive index of the solvent, the gradient of straight line, and quantum yield. Subscripts r and x indicate the reference solution and the tested samples, respectively. For the measurement, the wavelength of excitonic absorption peak of the resultant SiNPs was the same as the excitation wavelength.

Photostability Comparison of FITC, CdTe QDs, CdSe/ZnS QDs, and SiNPs. CdTe QDs were synthesized based on previously reported microwave-assisted methods.[27−29] For guaranteeing a reliable comparison, the photoluminescence intensities of all the samples were set as the same value. Continuous

irradiation was imposed by using a 365 nm UV lamp with a power of 450 W.

Cell Viability Measurement through MTT Assay. An array of 96-well plates was used for dispersing the Hela cells; 1×10^4 cells and 10 μL of SiNPs whose concentrations are equal to those used for cellular imaging were contained in each well. After incubation in a humidified atmosphere at 37 °C (5% CO_2) for serial hours (*e.g.*, 0.5, 3, 6, 12, 24, and 48 h), the cytotoxicity of the SiNPs was measured through the established MTT (3-(4,5-dimethylthiazol-2-yl)-2,5-diphenyltetrazolium bromide) assay. An ELISA reader was used for establishing a linear relationship between cell number and optical density, further enabling the calculation of the cell viability.

pH Stability of the As-Prepared SiNPs. The pH of the SiNPs aqueous solution was adjusted though dropwise addition of HCl or NaOH. A Seven Multi pH meter (Mettler Toledo) was utilized for monitoring the pH values, and meanwhile, a Horiba Jobin Yvon Fluoromax-4 spectrofluorimeter was used for recording the PL intensity fo the samples. The pH stability of SiNPs in Dulbecco's Modified Eagle Medium (DMEM) medium containing 10% Fetal Bovine Serum (FBS) at 37 °C was also measured.

SiNPs/Antibody Conjugation. The carboxylic acid groups of the protein were reacted with the amino groups of SiNPs in the presence of zero-length cross-linkers, that is, *N*-(3-(dimethylamino)propyl)-*N*-ethylcarbodiimde hydrochloride (EDC). For adequately activating the carboxylic acid, 2 μL of EDC (6.4 mg/mL in H_2O) was first incubated with 12.5 μL of goat antimouse IgG (4 mg/mL) in PBS buffer for 15 min at 25 °C. Afterward, the activated goat antimouse IgG was further incubated with 110 μL of green-emitting SiNPs (absorption value, 0.3; λ_{abs}, 345 nm) for 2 h at 25 °C, and then shaken in the dark for overnight at 4 °C. Nanosep centrifugal devices (300 kDa) were used for filtrating the isourea byproduct and residual reagent through centrifugation treatment (5000 rmp, 15 min). The produced SiNPs-IgG in the upper phase was finally diluted using 30 μL of PBS (pH = 7.4, 0.1 M) buffer and stored at 4 °C in the dark for the following cellular imaging experiment.

Long-Term Cellular Imaging. Dulbecco's modified Eagle's medium (DMEM) with 10% heat-inactivated fetal bovine serum (FBS) and antibiotics (100 μg/mL streptomycin and 100 U/mL penicillin) were used for culturing human epithelial cervical cancer cells (Hela cells) on a cover glass overnight. Sucrose (4%) and paraformaldehyde (4%) were utilized for fixing Hela cells, and PBS containing 4% BSA and 0.1% Triton X-100 was then used for blocking, followed by washing with PBS containing 0.1% Tween20 for three times. For labeling microtubules, the resultant Hela cells were then sequentially incubated with monoclonal anti-α-tubulin for 1 h and the SiNPs-IgG for 1 h. Thereafter, slides in Fluoromount (sigma, F4680) were used for mounting the stained cells, which were ready for examination through a confocal laser microscope (Leica, TCS-SP5). For CdTe QDs or FITC, all procedures were the same as those mentioned above. In our experiment, 15% power of argon laser and 3% power of diode laser were used, since the power values of these two laser sources were similar. Windows for FITC, QDs, SiNPs, and Hoechst are 515−545 nm, 570−670 nm, 500−600 nm, and 415−485 nm, respectively. A cooled CCD camera was used for capturing images at 40 s intervals. Microtubules labeled by FITC, CdTe QDs, or SiNPs were excited by argon laser ($\lambda_{excitation}$ = 488 nm, 100 mW); 15% power of the argon laser was used in our experiment. Windows for FTIC, CdTe QDs, and SiNPs are 515−545 nm, 570−670 nm, and 500−600 nm, respectively. Other experimental conditions were the same in comparison experiments. A cooled CCD camera was used for capturing each image at 15 s intervals.

Conflict of Interest: The authors declare no competing financial interest.

Supporting Information Available: Figure S1−25 and corresponding discussion. Comparison of method to prior work. The Supporting Information is available free of charge on the ACS Publications website at DOI: 10.1021/acsnano.5b00683.

Acknowledgment. The authors thank the National Basic Research Program of China (973 Program 2013CB934400 and 2012CB932400), the National Natural Science Foundation of China (Grant No. 61361160412 and 31400860), the Natural Science Foundation of Jiangsu Province of China (Grant No. BK20130052 and BK20130298), the Six Talent Peaks Project of Jiangsu Province (Gran No. 2013-XCL-036), a project funded by the Priority Academic Program Development of Jiangsu Higher Education Institutions (PAPD) and Collaborative Innovation Center of Suzhou Nano Science and Technology (NANO−CIC) for financial support.

REFERENCES AND NOTES

1. Pavesi, L.; Negro, L. D.; Mazzoleni, C.; Franzo, G.; Priolo, F. Optical Gain in Silicon Nanocrystals. *Nature* **2000**, *408*, 440–444.
2. Ding, Z. F.; Quinn, B. M.; Haram, S. K.; Pell, L. E.; Korgel, B. A.; Bard, A. J. Electrochemistry and Electrogenerated Chemiluminescence from Silicon Nanocrystal Quantum Dots. *Science* **2002**, *296*, 1293–1297.
3. Grom, G. F.; Lockwood, D. J.; McCaffrey, J. P.; Labbé, H. J.; Fau-chet, P. M., Jr; B, W.; Diener, J.; Kovalev, D.; Koch, F.; Tsybeskov, L. Ordering and Self-Organization in Nanocrystalline Silicon. *Nature* **2000**, *407*, 358–361.
4. Gu, L.; Hall, D. J.; Qin, Z. T.; Anglin, E.; Joo, J.; Mooney, D. J.; Howell, S. B.; Sailor, M. J. *In Vivo* Time-Gated Fluorescence Imaging with Biodegradable Luminescent Porous Silicon Nanoparticles. *Nat. Commun.* **2013**, *4*, 2326.
5. Park, J. h.; Gu, L.; Maltzahn, G. V.; Ruoslahti, E.; Bhatia, S. N.; Sailor, M. J. Biodegradable Luminescent Porous Silicon Nanoparticles for *in Vivo* Applications. *Nat. Mater.* **2009**, *8*, 331–336.
6. He, Y.; Fan, C. H.; Lee, S. T. Silicon Nanostructures for Bioapplications. *Nano Today* **2010**, *5*, 282–295.
7. He, Y.; Su, Y. Y.; Yang, X. B.; Kang, Z. H.; Xu, T. T.; Zhang, R. Q.; Fan, C. H.; Lee, S. T. Photo and pH Stable, Highly-Luminescent Silicon Nanospheres and Their Bioconjugates for Immunofluorescent Cell Imaging. *J. Am. Chem. Soc.* **2009**, *131*, 4434–4438.
8. He, Y.; Zhong, Y. L.; Peng, F.; Wei, X. P.; Su, Y. Y.; Lu, Y. M.; Su, S.; Gu, W.; Liao, L. S.; Lee, S. T. One-Pot Microwave Synthesis of Water-Dispersible, Ultraphoto- and pH-Stable, and Highly Fluorescent Silicon Quantum Dots. *J. Am. Chem. Soc.* **2011**, *133*, 14192–14195.
9. Zhong, Y. L.; Peng, F.; Bao, F.; Wang, S. Y.; Ji, X. Y.; Yang, L.; Su, Y. Y.; Lee, S. T.; He, Y. Large-Scale Aqueous Synthesis of Fluorescent and Biocompatible Silicon Nanoparticles and Their Use as Highly Photostable Biological Probes. *J. Am. Chem. Soc.* **2013**, *135*, 8350–8356.
10. Ji, X. Y.; Peng, F.; Zhong, Y. L.; Su, Y. Y.; Jiang, X. X.; Song, C. X.; Yang, L.; Chu, B. B.; Lee, S. T.; He, Y. Highly Fluorescent, Photostable, and Ultrasmall Silicon Drug Nanocarriers for Long-Term Tumor Cell Tracking and *in-Vivo* Cancer Therapy. *Adv. Mater.* **2015**, *27*, 1029–1034.
11. Zhong, Y. L.; Peng, F.; Wei, X. P.; Zhou, Y. F.; Wang, J.; Jiang, X. X.; Su, Y. Y.; Su, S.; Lee, S. T.; He, Y. Microwave-Assisted Synthesis of Biofunctional and Fluorescent Silicon Nanoparticles Using Proteins as Hydrophilic Ligands. *Angew. Chem., Int. Ed.* **2012**, *51*, 8485–8489.
12. Mastronardi, M. L.; Hennrich, F.; Henderson, E. J.; Maier-Flaig, F.; Blum, C.; Reichenbach, J.; Lemmer, U.; Kübel, C.; Wang, D.; Kappes, M. M.; Ozin, G. A. Preparation of Monodisperse Silicon Nanocrystals Using Density Gradient Ultracentrifugation. *J. Am. Chem. Soc.* **2011**, *133*, 11928–11931.
13. Mastronardi, M. L.; Maier-Flaig, F.; Faulkner, D.; Henderson, E. J.; Kübel, C.; Lemmer, U.; Ozin, G. A. Size-Dependent Absolute Quantum Yields for Size-Separated Colloidally-Stable Silicon Nanocrystals. *Nano Lett.* **2012**, *12*, 337–342.
14. Howes, P. D.; Chandrawati, R.; Stevens, M. M. Colloidal Nanoparticles as Advanced Biological Sensors. *Science* **2014**, *346*, 6205.
15. Cheng, X. Y.; Lowe, S. B.; Reece, P. J.; Gooding, J. J. Colloidal Silicon Quantum Dots: From Preparation to the Modification of Self-Assembled Monolayers (SAMs) for Bio-applications. *Chem. Soc. Rev.* **2014**, *43*, 2680–2700.

16. McVey, B. F. P.; Tilley, R. D. Solution Synthesis, Optical Properties, and Bioimaging Applications of Silicon Nanocrystals. *Acc. Chem. Res.* **2014**, *47*, 3045–3051.
17. Peng, F.; Su, Y. Y.; Zhong, Y. L.; Fan, C. H.; Lee, S. T.; He, Y. Silicon Nanomaterials Platform for Bioimaging, Biosensing, and Cancer Therapy. *Acc. Chem. Res.* **2014**, *47*, 612–623.
18. Purkait, T. K.; Iqbal, M.; Wahl, M. H.; Gottschling, K.; Gonzalez, C. M.; Islam, M. A.; Veinot, J. G. C. Borane-Catalyzed Room-Temperature Hydrosilylation of Alkenes/Alkynes on Silicon Nanocrystal Surfaces. *J. Am. Chem. Soc.* **2014**, *136*, 17914–17917.
19. Lin, T.; Liu, X.; Zhou, B.; Zhan, Z. Y.; Cartwright, A. N.; Swihart, M. T. A Solution-Processed UV-Sensitive Photodiode Produced Using a New Silicon Nanocrystal Ink. *Adv. Funct. Mater.* **2014**, *24*, 6016–6022.
20. Mastronardi, M. L.; Henderson, E. J.; Puzzo, D. P.; Ozin, G. A. Small Silicon, Big Opportunities: The Development and Future of Colloidally-Stable Monodisperse Silicon Nanocrystals. *Adv. Mater.* **2012**, *24*, 5890–5898.
21. Ganguly, S.; Kazem, N.; Carter, D.; Kauzlarich, S. M. Colloidal Synthesis of an Exotic Phase of Silicon: The BC8 Structure. *J. Am. Chem. Soc.* **2014**, *136*, 1296–1299.
22. Ghosh, B.; Masuda, Y.; Wakayama, Y.; Imanaka, Y.; Inoue, J. I.; Hashi, K.; Deguchi, K.; Yamada, H.; Sakka, Y.; Ohki, S.; *et al*. Hybrid White Light Emitting Diode Based on Silicon Nanocrystals. *Adv. Funct. Mater.* **2014**, *24*, 7151–7160.
23. Erogbogbo, F.; Yong, K. T.; Roy, I.; Hu, R.; Law, W. C.; Zhao, W. W.; Ding, H.; Wu, F.; Kumar, R.; Swihart, M. T.; Prasad, P. N. *In Vivo* Targeted Cancer Imaging, Sentinel Lymph Node Mapping and Multi-channel Imaging with Biocompatible Silicon Nanocrystals. *ACS Nano* **2011**, *5*, 413–423.
24. Kornowski, A.; Giersig, M.; Vogel, R.; Chemseddine, A.; Weller, H. Nanometer-Sized Colloidal Germanium Particles: Wet-Chemical Synthesis, Laser-Induced Crystallization, and Particle Growth. *Adv. Mater.* **1993**, *5*, 634–636.
25. Baldwin, R. K.; Pettigrew, K. A.; Garno, J. C.; Power, P. P.; Liu, G. Y.; Kauzlarich, S. M. Room Temperature Solution Synthesis of Alkyl-Capped Tetrahedral Shaped Silicon Nanocrystals. *J. Am. Chem. Soc.* **2002**, *124*, 1150–1151.
26. Baldwin, R. K.; Pettigrew, K. A.; Ratai, E.; Augustine, M. P.; Kauzlarich, S. M. Solution Reduction Synthesis of Surface Stabilized Silicon Nanoparticles. *Chem. Commun.* **2002**, 1822–1823.
27. He, Y.; Lu, H. T.; Sai, L. M.; Lai, W. Y.; Fan, Q. L.; Wang, L. H.; Huang, W. Microwave-Assisted Growth and Characterization of Water-Dispersed CdTe/CdS Core−Shell Nanocrystals with High Photoluminescence. *J. Phys. Chem. B* **2006**, *110*, 13370–13374.
28. He, Y.; Lu, H. T.; Sai, L. M.; Lai, W. Y.; Fan, Q. L.; Wang, L. H.; Huang, W. Synthesis of CdTe Nanocrystals through Program Process of Microwave Irradiation. *J. Phys. Chem. B* **2006**, *110*, 13352–13356.
29. He, Y.; Lu, H. T.; Sai, L. M.; Su, Y. Y.; Hu, M.; Fan, C. H.; Huang, W.; Wang, L. H. Microwave Synthesis of Water-Dispersed CdTe/CdS/ZnS Core−Shell−Shell Quantum Dots with Excellent Photostability and Biocompatibility. *Adv. Mater.* **2008**, *20*, 3416–3421.
30. He, Y.; Zhong, Y. L.; Peng, F.; Wei, X. P.; Su, Y. Y.; Su, S.; Gu, W.; Liao, L. S.; Lee, S. T. Highly Luminescent Water-Dispersible Silicon Nanowires for Long-Term Immunofluorescent Cellular Imaging. *Angew. Chem., Int. Ed.* **2011**, *50*, 3080–3083.
31. Peng, F.; Su, Y. Y.; Wei, X. P.; Lu, Y. M.; Zhou, Y. F.; Zhong, Y. L.; Lee, S. T.; He, Y. Silicon-Nanowire-Based Nanocarriers with Ultrahigh Drug-Loading Capacity for *in Vitro* and *in Vivo* Cancer Therapy. *Angew. Chem., Int. Ed.* **2013**, *52*, 1457–1461.
32. Dasog, M.; Reyes, G. B. D. L.; Titova, L. V.; Hegmann, F. A.; Veinot, J. G. C. Size *vs* Surface: Tuning the Photoluminescence of Freestanding Silicon Nanocrystals across the Visible Spectrum *via* Surface Groups. *ACS Nano* **2014**, *8*, 9636–9648.
33. English, D. S.; Pell, L. E.; Yu, Z. H.; Barbara, P. F.; Korgel, B. A. Size Tunable Visible Luminescence from Individual Organic Monolayer Stabilized Silicon Nanocrystal Quantum Dots. *Nano Lett.* **2002**, *2*, 681–685.
34. Han, M. Y.; Özyilmaz, B.; Zhang, Y. B.; Kim, P. Energy Band-Gap Engineering of Grapheme Nanoribbons. *Phys. Rev. Lett.* **2007**, *98*, 206805.
35. Allan, G.; Delerue, C.; Lannoo, M. Nature of Luminescent Surface of Semiconductor Nanocrystallites. *Phys. Rev. Lett.* **1996**, *76*, 2961–2964.
36. Zhou, Z. Y.; Brus, L.; Friesner, R. Electronic Structure and Luminescence of 1.1- and 1.4-nm Silicon Nanocrystals: Oxide Shell *versus* Hydrogen Passivation. *Nano Lett.* **2003**, *3*, 163–167.
37. Puzder, A.; Williamson, A. J.; Grossman, J. C.; Galli, G. Computational Studies of the Optical Emission of Silicon Nanocrystals. *J. Am. Chem. Soc.* **2003**, *125*, 2786–2791.
38. Dukovic, G.; Wang, F.; Song, D. H.; Sfeir, M. Y.; Heinz, R. F.; Brus, L. E. Structural Dependence of Excitonic Optical Transitions and Band-Gap Energies in Carbon Nanotubes. *Nano Lett.* **2005**, *5*, 2314–2318.
39. Porezag, D.; Frauenheim, T.; Köhler, T. Construction of Tight-Binding-like Potentials on The Basis of Density-Functional Theory: Application to Carbon. *Phys. Rev. B* **1995**, *51*, 12947.
40. Niehaus, T. A.; Suhai, S. Tight-Binding Approach to Time-Dependent Density-Functional Response Theory. *Phys. Rev. B* **2001**, *63*, 085108.
41. Li, Q. S.; Zhang, R. Q.; Niehaus, T. A.; Frauenheim, T.; Lee, S. T. Theoretical Studies on Optical and Electronic Properties of Propionic-Acid-Terminated Silicon Quantum Dots. *J. Chem. Theory Comput.* **2007**, *3*, 1518–1526.
42. Li, Q. S.; Zhang, R. Q.; Lee, S. T.; Niehaus, T. A.; Frauenheim, T. Amine-Capped Silicon Quantum Dots. *Appl. Phys. Lett.* **2008**, *92*, 053107.
43. Su, Y. Y.; Peng, F.; Jiang, Z. Y.; Zhong, Y. L.; Lu, Y. M.; Jiang, X. X.; Huang, Q.; Fan, C. H.; Lee, S. T.; He, Y. *In vivo* Distribution, Pharmacokinetics, and Toxicity of Aqueous Synthesized Cadmium-Containing Quantum Dots. *Biomaterials* **2011**, *32*, 5855–5862.
44. He, Y.; Lu, H. T.; Su, Y. Y.; Sai, L. M.; Hu, M.; Fan, C. H.; Wang, L. H. Ultra-photostable, Non-cytotoxic, and Highly Fluorescent Quantum Nanospheres for Long-Term, High-Specificity Cell Imaging. *Biomaterials* **2011**, *32*, 2133–2140.
45. Lu, Y. M.; Su, Y. Y.; Zhou, Y. F.; Wang, J.; Peng, F.; Zhong, Y. L.; Huang, Q.; Fan, C. H.; He, Y. *In Vivo* Behavior of Near-Infrared-Emitting Quantum Dots. *Biomaterials* **2013**, *34*, 4302–4308.
46. Alivisatos, A. P. Semiconductor Clusters, Nanocrystals, and Quantum Dots. *Science* **1996**, *271*, 933–937.
47. Holmes, J. D.; Ziegler, K. J.; Doty, R. C.; Pell, L. E.; Johnston, K. P.; Korgel, B. A. Highly Luminescent Silicon Nanocrystals with Discrete Optical Transitions. *J. Am. Chem. Soc.* **2001**, *123*, 3743–3748.
48. Park, N. M.; Choi, C. J.; Seong, T. Y.; Park, S. J. Quantum Confinement in Amorphous Silicon Quantum Dots Embedded in Silicon Nitride. *Phys. Rev. Lett.* **2001**, *86*, 1355–1357.
49. Allan, G.; Delerue, C.; Lannoo, M. Nature of Luminescent Surface States of Semiconductor Nanocrystallites. *Phys. Rev. Lett.* **1996**, *76*, 2961–2964.
50. Cullis, A. G.; Canham, L. T. Visible Light Emission Due to Quantum Size Effects in Highly Porous Crystalline Silicon. *Nature* **1991**, *353*, 335–338.
51. Wilcoxon, J. P.; Samara, G. A.; Provencio, P. N. Optical and Electronic Properties of Si Nanoclusters Synthesized in Inverse Micelles. *Phys. Rev. B* **1999**, *60*, 2704–2714.
52. Takagahara, T.; Takeda, K. Theory of The Quantum Confinement Effect on Excitons in Quantum Dots of Indirect-Gap Materials. *Phys. Rev. B* **1992**, *46*, 15578–15581.
53. Augustine, B. H.; Irene, E. A. Visible Light Emission from Thin Films Containing Si, O, N, and H. *J. Appl. Phys.* **1995**, *78*, 4020–4030.
54. Chang, M. C.; Tanaka, J. FT-IR Study for Hydroxyapatite/Collagen Nanocomposite Cross-Linked by Glutaraldehyde. *Biomaterials* **2002**, *23*, 4811–4818.
55. Schwanninger, M.; Rodrigues, J. C.; Pereira, H.; Hinterstoisser, B. Effects of Short-Time Vibratory Ball Milling on The Shape of FT-IR Spectra of Wood and Cellulose. *Vib. Spectrosc.* **2004**, *36*, 23–40.

56. Dancil, K. P. S.; Greiner, D. P.; Sailor, M. J. A Porous Silicon Optical Biosensor: Detection of Reversible Binding of IgG to Protein A-Modified Surface. *J. Am. Chem. Soc.* **1999**, *121*, 7925–7930.
57. Hamers, R. J.; Coulter, S.; Ellison, M. D.; Hovis, J. S.; Padowitz, D. F.; Schwartz, M. P. Cycloaddition Chemistry of Organic Molecules with Semiconductor Surfaces. *Acc. Chem. Res.* **2000**, *33*, 617–624.
58. El-Sayed, M. Y.; Refat, M. S. The Intermolecular Charge-Transfer Complexes of The First Generation of Ploy-(propylene amine) Dendrimers with σ and π Acceptors. *Int. J. Electrochem. Sci.* **2014**, *9*, 6608–6626.
59. Grabchev, I.; Bojinov, V.; Petkov, C. Infrared Absorption Studies of Some New 1,8-Naphthalimides. *Chem. Heterocycl. Compd.* **2003**, *39*, 179–183.
60. Grab-chev, I.; Petkov, C.; Bojinov, V. 1,8-Naphthalimides as Blue Emitting Fluorophores for Polymer Materials. *Macromol. Mater. Eng.* **2002**, *287*, 904–908.
61. He, Y.; Zhong, Y. L.; Su, Y. Y.; Lu, Y. M.; Jiang, Z. Y.; Peng, F.; Xu, T. T.; Su, S.; Huang, Q.; Fan, C. H.; Lee, S. T. Water-Dipersed Near-Infrared-Emitting Quantum Dots of Ultrasmall Sizes for *in Vitro* and *in Vivo* Imaging. *Angew. Chem., Int. Ed.* **2011**, *50*, 5695–5698.
62. Gaponik, N.; Talapin, D. V.; Rogach, A. L.; Hoppe, K.; Shevchenko, E. V.; Kornowski, A.; Eychmüller, A.; Weller, H. Thiol-Capping of CdTe Nanocrystals: An Alternative to Organometallic Synthetic Routes. *J. Phys. Chem. B* **2002**, *106*, 7177–7185.
63. Kirchner, C.; Liedl, T.; Kudera, S.; Pellegrino, T.; Javier, A. M.; Gaub, H. E.; Stölzle, S.; Fertig, N.; Parak, W. J. Cytotoxicity of Colloidal CdSe and CdSe/ZnS Nanoparticles. *Nano Lett.* **2005**, *5*, 331–338.
64. Wang, S. P.; Mamedova, N.; Kotov, N. A.; Chen, W.; Studer, J. Antigen/Antibody Immunocomplex from CdTe Nanoparticle Bioconjugates. *Nano Lett.* **2002**, *2*, 817–822.
65. Xing, Y.; Chaudry, Q.; Shen, C.; Kong, K. Y.; Zhau, H. E.; Chung, L. W.; Petros, J. A.; O'Regan, R. M.; Yezhelyev, M. V.; Simons, J. W.; *et al*. Bioconjugated Quantum Dots for Multiplexed and Quantitative Immunohistochemistry. *Nat. Protoc.* **2007**, *2*, 1152–1165.
66. Ma, D. D. D.; Lee, C. S.; Au, F. C. K.; Tong, S. Y.; Lee, S. T. Small-Diameter Silicon Nanowire Surfaces. *Science* **2003**, *299*, 1874–1877.
67. Allen, J. E.; Hemesath, E. R.; Perea, D. E.; Lensch-falk, J. L.; Li, Z. Y.; Yin, F.; Gass, M. H.; Wang, P.; Bleloch, A. L.; Palmer, R. E.; *et al*. High-Resolution Detection of Au Catalyst Atoms in Si Nanowires. *Nat. Nanotechnol.* **2008**, *3*, 168–173.
68. Patolsky, F.; Timko, B. P.; Yu, G. H.; Fang, Y.; Greytak, A. B.; Zheng, G. F.; Lieber, C. M. Detection, Stimulation, and Inhibition of Neuronal Signals with High-Density Nanowire Transistor Arrays. *Science* **2006**, *313*, 1100–1104.
69. He, Y.; Sai, L. M.; Lu, H. T.; Hu, M.; Lai, W. Y.; Fan, Q. L.; Wang, L. H.; Huang, W. Microwave-Assisted Synthesis of Water-Dispersed CdTe Nanocrystals with High Luminescent Efficiency and Narrow Size Distribution. *Chem. Mater.* **2007**, *19*, 359–365.